2005 International Linear Collider Workshop - Stanford, U.S.A.

Effects of the $t\bar{t}$ Threshold in $e^+e^- \to t\bar{t}H$

C. Farrell, A.H. Hoang
Max-Planck-Institut for Physics, Munich, Germany

In the region where the Higgs energy is large the process $e^+e^- \to t\bar{t}H$ is governed by nonrelativistic QCD dynamics and one has to employ effective theory methods to make first principles QCD predictions. In this talk we use the effective theory vNRQCD to compute the Higgs energy distribution at next-to-leading logarithmic approximation. It is shown that the corrections are particularly important for smaller c.m. energies.

1. INTRODUCTION

It is one of the major tasks of future collider experiments to unravel details of the mechanism of electroweak symmetry breaking (EWSB). In the Standard Model (SM) EWSB is achieved by the Higgs mechanism. The particle masses are generated by the Higgs field vacuum expectation value $V = (\sqrt{2}\,G_F)^{1/2} \approx 246$ GeV arising through the Higgs self interactions. The mechanism also predicts that Higgs bosons can be produced in collider experiments. While a Higgs boson with a mass smaller than 1 TeV can be found at the LHC, precise and model-independent measurements of its quantum numbers and couplings can be gained from the e^+e^- Linear Collider. A crucial prediction of the Higgs mechanism is that the Higgs Yukawa coupling to quarks λ_q is related to the quark masses by $m_q = \lambda_q V$. At the e^+e^- Linear Collider the top quark Yukawa coupling can be measured from top quark pair production associated with a Higgs boson, $e^+e^- \to t\bar{t}H$, since the process is dominated by the amplitudes describing Higgs radiation off the $t\bar{t}$ pair. This process is particularly suited for a light Higgs boson since the cross section can then reach the 1-2 fb level. Assuming an experimental precision at the percent level, QCD and electroweak radiative corrections need to be accounted for in the theoretical predictions. In the approximation that top quarks and the Higgs are stable particles the Born cross section was already determined some time ago in Refs. [1]. For the $\mathcal{O}(\alpha_s)$ QCD one-loop corrections a number of references in various approximations exist [2–4]. On the other hand, the full set of one-loop electroweak corrections was obtained in Refs. [5, 6] and also in Refs. [7]. In Ref. [6] a detailed analysis of various differential distributions of the cross section $\sigma(e^+e^- \to t\bar{t}H)$ can be found.

A particularly interesting kinematical phase space region is where the energy of the Higgs boson is large and close to its kinematic endpoint. The $t\bar{t}$ pair then becomes collinear and flies opposite to the Higgs direction to balance the large Higgs momentum, see Fig. 1. For large E_H, on the other hand, the $t\bar{t}$ invariant mass Q^2 approaches $4m_t^2$, $E_H = \frac{1}{2\sqrt{s}}\left(s + m_H^2 - Q^2\right)$, and the top quark pair is nonrelativistic in its own center-of-mass (c.m.) system. Because the Higgs is very narrow for a mass below the W^+W^- threshold, strong interactions between the $t\bar{t}$ pair and the hadronic Higgs final state can be neglected. Thus, close to the Higgs energy endpoint the $t\bar{t}$ QCD dynamics is exclusively governed by the nonrelativistic physics known from the process $e^+e^- \to t\bar{t}$ in the $t\bar{t}$ threshold region at $\sqrt{s} \approx 2m_t$. In this regime the so-called Coulomb singularities $\propto (\alpha_s/v)^n$, with $v = (1 - 4m_t^2/Q^2)^{1/2}$ being the top quark relative velocity in the $t\bar{t}$ c.m. frame, arise and require predictions using an expansion in α_s and v rather than just a perturbative computation in the number of loops.

This singularity structure is most easily visible in the Higgs energy distribution, $d\sigma(e^+e^- \to t\bar{t}H)/dE_H$. While the Born distribution approaches zero for $E_H \to E_H^{\rm max}$, $d\sigma/dE_H \sim v$ [1], the $\mathcal{O}(\alpha_s)$ fixed-order perturbative corrections are proportional to α_s at the endpoint [3, 4] and the $\mathcal{O}(\alpha_s^2)$ corrections even diverge like α_s^2/v. The problem might be avoided by imposing a cut on E_H or Q^2, but this is unnecessary because there exists an elaborate technology being used for the threshold region in the process $e^+e^- \to t\bar{t}$ [8] that allows for systematic QCD predictions with renormalization group (RG) improvement. Imposing a cut would be also disadvantageous as the nonrelativistic portion of the $t\bar{t}H$ phase space increases for smaller c.m. energies which are relevant for a measurement in the first

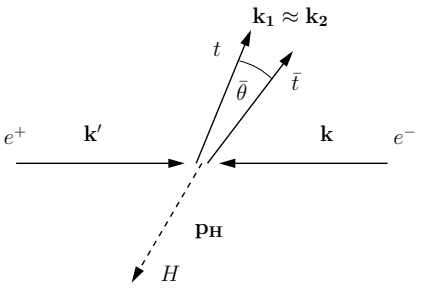

Figure 1: Typical constellation of momenta for the process $e^+e^- \to t\bar{t}H$ in the large Higgs energy endpoint region.

phase of the ILC program. Because the SM top width is quite large, $\Gamma_t \approx 1.5$ GeV, the corresponding QCD effective theory computations can be carried out with perturbative methods for all Higgs energies in the endpoint region.

In this talk we present the Higgs energy distribution $d\sigma/dE_H$ in the large Higgs energy endpoint region at NLL order in the nonrelativistic expansion using the framework of "velocity" NRQCD (vNRQCD). For details on the conceptual aspects, concerning powercounting, the operator structure of the effective theory action, and renormalization we refer to Refs. [10–14]. For a more detailed discussion of the computations for this work see Ref. [9].

2. REVIEW OF EFFECTIVE THEORY INGREDIENTS

The effective theory vNRQCD provides a systematic RG-improved description of dynamics of nonrelativistic $t\bar{t}$ pairs. The system is characterized, for any energy in the threshold region, by the hierarchy

$$m_t \gg m_t v \text{ (three-momentum, "soft" scale)} \gg m_t v^2 \text{ (kinetic energy, "ultrasoft" scale)} \gg \Lambda_{\rm QCD}\,. \tag{1}$$

The particle-antiparticle propagation is described by the terms in the effective theory Lagrangian which are bilinear in the top quark and antitop quark fields,

$$\mathcal{L}(x) \;=\; \sum_{\boldsymbol{p}} \psi^\dagger_{\boldsymbol{p}}(x)\Big\{ i\partial^0 - \frac{\boldsymbol{p}^2}{2m_t} + \frac{i}{2}\Gamma_t - \delta m_t \Big\}\psi_{\boldsymbol{p}}(x) + (\psi_{\boldsymbol{p}}(x) \to \chi_{\boldsymbol{p}}(x))\,, \tag{2}$$

where the fields $\psi_{\boldsymbol{p}}$ and $\chi_{\boldsymbol{p}}$ destroy top and antitop quarks with soft three-momentum $\boldsymbol{p}$ in the $t\bar{t}$ c.m. frame and Γ_t is the on-shell top quark decay width. The term δm_t is a residual mass term specific to the top quark mass definition that is being used; for our analysis we employ the 1S mass scheme [15, 16].

Up to NLL order the top-antitop quark pair interacts only through the effective Coulomb potential [18],

$$\tilde{V}_c(\boldsymbol{p},\boldsymbol{q}) \;=\; -\frac{4\pi C_F \alpha_s(m_t\nu)}{\boldsymbol{k}^2}\,\left\{1 + \frac{\alpha_s(m_t\nu)}{4\pi}\,\left[-\beta_0\,\ln\Big(\frac{\boldsymbol{k}^2}{m_t^2\nu^2}\Big) + a_1\right]\right\}\,, \tag{3}$$

where $\boldsymbol{k} = \boldsymbol{p} - \boldsymbol{q}$ is the momentum transfer and $\beta_0 = 11/3C_A - 4/3Tn_f$ is the one-loop QCD beta function, $a_1 = 31/9C_A - 20/9Tn_f$ the coefficient of the one-loop correction to the effective Coulomb potential, and $C_A = 3, C_F = 4/3, T = 1/2$ are SU(3) group theoretical factors. For the number of light flavors we take $n_f = 5$. The parameter ν is the vNRQCD renormalization scaling parameter used to describe the correlated running of soft and ultrasoft effects in the effective theory. Here, $\nu = 1$ corresponds to the hard scale at which the effective theory is matched to the full theory, and $\nu = v_0$, v_0 being of the order of the typical $t\bar{t}$ relative velocity, is the scale where the matrix elements are computed. The evolution of the Wilson coefficients from the matching scale down to the low-energy scale sums logarithms of the velocity to all orders and is governed by the velocity renormalization group equations [10].

Top-antitop quark production in the nonrelativistic regime in the LL and NLL approximation in a ${}^3S_1$ spin triplet or a ${}^1S_0$ spin singlet state is described by the currents

$$J^j_{1,\boldsymbol{p}} = \psi^\dagger_{\boldsymbol{p}}\,\sigma_j(i\sigma_2)\chi^*_{-\boldsymbol{p}}\,, \qquad\qquad J_{0,\boldsymbol{p}} = \psi^\dagger_{\boldsymbol{p}}\,(i\sigma_2)\chi^*_{-\boldsymbol{p}}\,, \tag{4}$$

where $c_{1,j}(\nu)$ and $c_0(\nu)$ are the corresponding Wilson coefficients. The currents do not run at LL order but UV-divergences in effective theory two-loop vertex diagrams [10] lead to non-trivial anomalous dimensions at NLL order which result in a scaling of the Wilson coefficients [13, 19]

$$c_{1,j}(\nu) = c_{1,j}(1)\,\exp\big(f(\nu,\mathbf{S^2}=2)\big)\,, \qquad\qquad c_0(\nu) = c_0(1)\,\exp\big(f(\nu,\mathbf{S^2}=0)\big)\,, \tag{5}$$

where $\mathbf{S^2}$ is the square of the total $t\bar{t}$ spin. We have adopted the convention that the matching conditions at $\nu = 1$ only account for QCD effects, so at LL order we have $c_1(1) = c_0(1) = 1$. The NLL order QCD matching conditions relevant for $e^+e^- \to t\bar{t}H$ in the large Higgs energy endpoint region are discussed in Sec. 3.

Through the optical theorem the $t\bar{t}$ production rate for a $t\bar{t}$ invariant mass $Q^2 \approx 4m_t^2$ involves the imaginary part of the time-ordered product of the production and annihilation currents defined in Eqs. (4),

$$\mathcal{A}_1^{lk}(Q^2,m_t,\nu) \;=\; i\sum_{\boldsymbol{p},\boldsymbol{p'}}\int d^4x\,e^{-i\hat{q}\cdot x}\,\Big\langle\,0\,\Big|\,T\,J^{l\dagger}_{1,\boldsymbol{p'}}(0)J^k_{1,\boldsymbol{p}}(x)\Big|\,0\,\Big\rangle \;=\; 2N_c\delta^{lk}\,G^c(a,v,m_t,\nu)\,, \tag{6}$$

$$\mathcal{A}_0(Q^2,m_t,\nu) \;=\; i\sum_{\boldsymbol{p},\boldsymbol{p'}}\int d^4x\,e^{-i\hat{q}\cdot x}\,\Big\langle\,0\,\Big|\,T\,J^{\dagger}_{0,\boldsymbol{p'}}(0)J_{0,\boldsymbol{p}}(x)\Big|\,0\,\Big\rangle \;=\; N_c\,G^c(a,v,m_t,\nu)\,, \tag{7}$$

where $v = ((\sqrt{Q^2}-2m_t-2\delta m_t+i\Gamma_t)/m_t)^{\frac{1}{2}}$ is the c.m. top quark (effective) relative velocity and $\hat{q} \equiv (\sqrt{Q^2}-2m_t,0)$. The term G^c is the zero-distance S-wave Coulomb Green function of the nonrelativistic Schrödinger equation with the potential in Eq. (3). To compute the Green function we use the numerical techniques and codes of the TOPPIC program developed in Ref. [20] and determine an exact solution of the full NLL Schrödinger equation following the approach of Refs. [14].

3. COMMENTS ON THE COMPUTATION

The LL vNRQCD result for the Higgs energy distribution, including the QCD effects coming from the Coulomb potential in Eq. (3), the finite top quark lifetime, and the Wilson coefficients of the currents in Eqs. (5), is given by

$$\frac{d\sigma}{dE_H}(E_H \approx E_H^{\rm max}) \;=\; \frac{8\,N_c\,\left[(1+x_H-4x_t)^2-4x_H\right]^{1/2}}{s^{3/2}\,m_t^2}\,\Big(\,c_0^2(\nu)\,F_0^Z + c_1^2(\nu)\,F_1^{\gamma,Z}\,\Big)\;{\rm Im}\,[\,G^c(a,v,m_t,\nu)\,]\;. \tag{8}$$

For details on the explicit calculation and the definition of the formfactors F_i see [9]. We note that the NLL ($\mathcal{O}(\alpha_s)$) matching conditions for the three triplet Wilson coefficients $c_{1,j}$ depend on the $t\bar{t}$ spin configuration (i.e. on j) since the kinematic situation for $t\bar{t}H$ production in the large Higgs energy endpoint is not invariant under separate rotations of the spin quantization axis. However, for our purposes it is sufficient to define a triplet Wilson coefficient that is averaged over the three spin configurations. Using such an averaged triplet Wilson coefficient the Higgs energy spectrum at NLL order can also be cast in the simple form of Eq. (8).

At NLL order, we need to account for the $\mathcal{O}(\alpha_s^2)$ contributions to the Coulomb potential in Eq. (3), the NLL running of the coefficients c_1 and c_0, and their $\mathcal{O}(\alpha_s)$ matching conditions at $\nu = 1$. The latter hard QCD corrections are process specific and cannot be inferred from results obtained in earlier computations for the $t\bar{t}$ threshold in $e^+e^- \to t\bar{t}$. We have extracted the matching conditions from the codes for the Standard Model amplitude for $e^+e^- \to t\bar{t}H$ provided in Ref. [6]. With the ansatz

$$c_{0,1}(\nu=1,\sqrt{s},m_t,m_H) = 1 + \frac{C_F\alpha_s(m_t)}{\pi}\,\delta c_{0,1}(\sqrt{s},m_t,m_H) \tag{9}$$

we have determined the $\mathcal{O}(\alpha_s)$ matching conditions numerically by matching the $\mathcal{O}(\alpha_s)$ vNRQCD prediction at $\mu = m_t$ ($\nu = 1$) to the full theory results close to the large Higgs energy endpoint. The relative uncertainties for this numerical procedure are below 1% for $\delta c_{0,1}$.

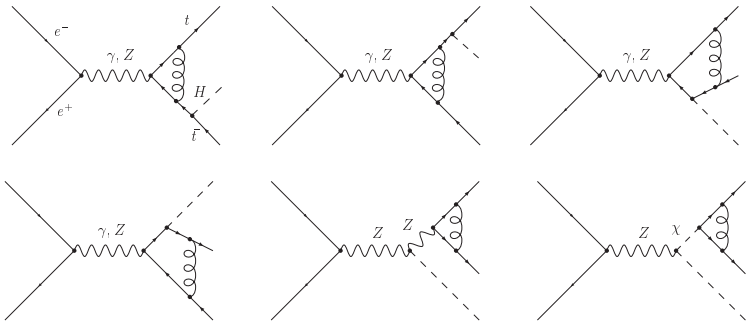

Figure 2: Diagrams describing virtual one-loop QCD corrections in the Standard Model to compute the NLL matching conditions for the operators $J_{1,\boldsymbol{p}}$ and $J_{0,\boldsymbol{p}}$ that describe $t\bar{t}$ production for invariant masses $Q^2 \approx 4m_t^2$. Self energy diagrams are implied.

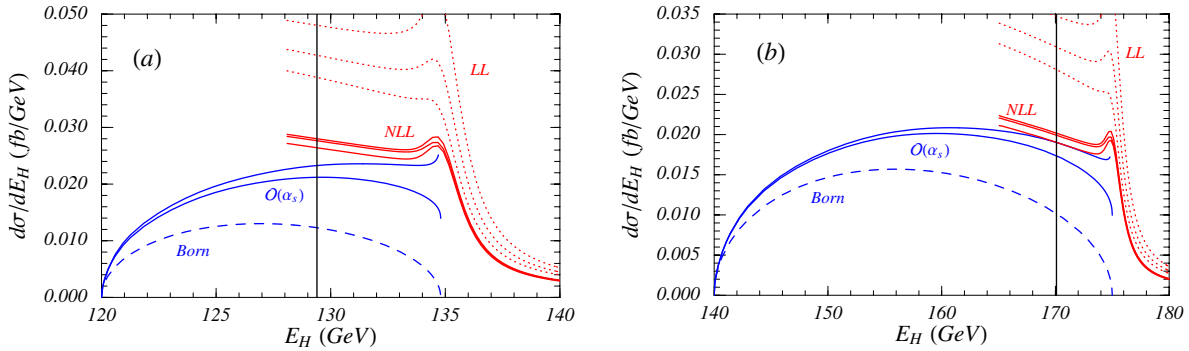

Figure 3: Higgs energy spectrum at LL (dotted lines) and NLL (solid lines) order in the nonrelativistic expansion for the vNRQCD renormalization parameters $\nu = 0.1, 0.2, 0.4$ and at the Born level and at $\mathcal{O}(\alpha_s)$ for $\mu = \sqrt{s}, \sqrt{s}|v|$ for the parameters (a) $\sqrt{s} = 500$ GeV, $m_H = 120$ GeV and (b) $\sqrt{s} = 550$ GeV, $m_H = 140$ GeV. The top 1S mass has been set to $m_t^{1S} = 180$ GeV and the other parameters are $\Gamma_t = 1.55$ GeV, $M_Z = 91.1876$ GeV, $M_W = 80.423$ GeV, $c_w = M_W/M_Z$ and $\alpha^{-1} = 137.034$.

4. NUMERICAL ANALYSIS

In Figs. 3 the predictions of the Higgs energy spectrum in the full kinematic range are displayed for two cases. In the large Higgs energy endpoint region we have shown the LL (dashed lines) and NLL (solid lines) results in the nonrelativistic expansion. (See the figure captions for details on choice of parameters.) At LL order the upper (lower) curve corresponds to $\nu = 0.1$ (0.4), while at NLL order the upper (lower) curve corresponds to $\nu = 0.2$ (0.1). The curves show the typical behavior of the prediction of the nonrelativistic expansion for any choice of parameters. While the LL predictions have a quite large renormalization parameter dependence at the level of several tens of percent, the NLL results are stable. Here, the variation due to change of the renormalization parameter is around 5%. The stabilization with respect to renormalization parameter variations at NLL order arises mainly from the inclusion of the $\mathcal{O}(\alpha_s)$ QCD corrections to the Coulomb potential, Eq. (3). Moreover, the NLL curves lie considerably lower than the LL ones. This behavior is well known from the predictions for $e^+e^- \to t\bar{t}$ at threshold [8, 14] and originates from the structure of the large negative $\mathcal{O}(\alpha_s)$ QCD corrections to the Coulomb potential, Eq. (3), and from the sizeable negative QCD corrections to the matching conditions in Eq. (9).

In principle this behavior is a point of concern because it could indicate that the renormalization parameter variation might be an inadequate method to estimate theoretical uncertainties. Fortunately, the top quark mass is sufficiently large such that the regions where the conventional fixed-order expansion (in powers of the strong coupling) and where the nonrelativistic expansion (described by the effective theory) can be applied are expected to overlap.

$\sqrt{s}$ [GeV]	m_H [GeV]	σ(Born) [fb]	$\sigma(\alpha_s)$ [fb]	σ(NLL) [fb]	$\frac{\sigma(\mathrm{NLL})}{\sigma(\mathrm{Born})}$	$\frac{\sigma(\mathrm{NLL})}{\sigma(\alpha_s)}$	$\frac{\sigma(\mathrm{NLL})_{\lvert\beta\rvert<0.2}}{\sigma(\alpha_s)_{\beta<0.2}}$
500	120	0.151	0.263	0.357(20)	2.362	1.359	1.78
550	120	0.984	1.251	1.342(37)	1.364	1.073	1.66
550	160	0.134	0.207	0.254(12)	1.902	1.226	1.74
600	120	1.691	1.939	2.005(30)	1.185	1.034	1.66
600	160	0.565	0.700	0.745(18)	1.319	1.065	1.68
700	120	2.348	2.454	2.485(13)	1.058	1.012	1.68
700	160	1.210	1.303	1.328(11)	1.098	1.020	1.69

Table I: Collection of cross sections and K factors for various c.m. energies and Higgs masses and top quark mass $m_t^{1S} = 180$ GeV. Here, σ(Born) refers to the Born cross section and $\sigma(\alpha_s)$ to the $\mathcal{O}(\alpha_s)$ cross section in fixed-order perturbation theory using $\mu = \sqrt{s}$ as the renormalization scale, the choice employed in the analysis of Ref. [6]. The term σ(NLL) refers to the sum of the $\mathcal{O}(\alpha_s)$ fixed-order cross section for $v > 0.2$ using $\mu = \sqrt{s}v$ and the NLL nonrelativistic cross section for $|v| < 0.2$ with the renormalization parameter $\nu = 0.2$. (See Figs. 3 where the vertical lines indicate the Higgs energy where $v = 0.2$.)

To demonstrate this issue we have also displayed in Figs. 3 the fixed-order (i.e. without summation of Coulomb singularities) predictions at the Born (dashed lines) [2] and the $\mathcal{O}(\alpha_s)$ level (solid lines) [6]. The two $\mathcal{O}(\alpha_s)$ curves correspond to the renormalization scales $\mu = \sqrt{s}$ (lower curves) and $\mu = |\sqrt{s}v|$ (upper curves), where v is the $t\bar{t}$ relative velocity defined below Eq. (7). The latter choice for the fixed-order renormalization scale is motivated by the fact that the relative momentum of the top pair is the scale governing the Coulomb singularities contained in the fixed-order expansion close to the large Higgs energy endpoint. This choice for the fixed-order renormalization scale is therefore the more appropriate one near the Higgs energy endpoint. The results in Figs. 3 demonstrate the overlap between the $\mathcal{O}(\alpha_s)$ fixed-order prediction and the NLL nonrelativistic one in the region where the $t\bar{t}$ relative velocity is approximately 0.2. (The Higgs energy with $v = 0.2$ is indicated in each panel by the solid vertical line.) The overlap improves for increasing c.m. energies or decreasing Higgs masses. This indicates that in the overlap regions the higher order contributions summed in the nonrelativistic prediction and the higher order relativistic corrections contained in the fixed-order result are both small. For smaller c.m. energies or increasing Higgs masses, on the other hand, the NLL nonrelativistic predictions tend to lie slightly above the $\mathcal{O}(\alpha_s)$ fixed-order results (for $\mu = \sqrt{s}v$) illustrating the impact of the higher order corrections to each type of expansion. The discrepancy, however, remains comparable to the uncertainties estimated from the renormalization parameter variation of the NLL nonrelativistic prediction. We therefore conclude that the renormalization parameter variation of the NLL order nonrelativistic prediction should provide a realistic estimate of the theoretical uncertainties in the large Higgs energy region. The results in Figs. 3 also demonstrate that the region of parameter space where the top quark pair is nonrelativistic increases for smaller c.m. energies (or larger Higgs masses).

Let us now discuss the numerical impact of the nonrelativistic contributions in the large Higgs energy region on the total cross section. In Tab. I the importance of the summation of the Coulomb singularities and the logarithms of the top quark velocity is analyzed numerically for various choices of the c.m. energy and the Higgs mass. For all cases the top quark mass $m_t^{1S} = 180$ GeV is used and the other parameters are fixed as in Figs. 3. See the caption for details on the various entries. The numbers for σ(NLL), which are determined from combining the NLL nonrelativistic predictions in the Higgs energy end point for $|v| < 0.2$ with the fixed-order $\mathcal{O}(\alpha_s)$ prediction for smaller Higgs energies with $|v| > 0.2$, represent the currently most complete predictions for the total cross section of the process $e^+e^- \to t\bar{t}H$ as far as QCD corrections are concerned. For σ(NLL) we have also given our estimate for the theoretical error. For the fixed-order contribution ($v > 0.2$) we have estimated the uncertainty by taking the maximum of the shifts obtained from varying μ in the ranges $[\sqrt{s}, 2\sqrt{s}]$, $[\sqrt{s}, \sqrt{s}/2]$ and $[\sqrt{s}v, \sqrt{s}]$; for the nonrelativistic contribution in the end point we have assumed an uncertainty of 5% for all cases. For the numbers displayed in Tab. I both uncertainties were added linearly.

The results show that the enhancement of the cross section due to the summations in the large Higgs energy

region is particularly important for smaller c.m. energies and larger Higgs masses, when the portion of the phase space where the nonrelativistic expansion has to be applied is large. Here, the higher order summations contained in the nonrelativistic expansion can be comparable to the already sizeable $\mathcal{O}(\alpha_s)$ fixed-order corrections and enhance the cross section further. This is advantageous for top Yukawa coupling measurements for the lower c.m. energies accessible in the first phase of the ILC experiment. For higher c.m. energies the effect of the nonrelativistic summations of contributions from beyond $\mathcal{O}(\alpha_s)$ is less pronounced and decreases to the one-percent level for c.m. energies above 700 GeV. For all cases, except for very large c.m. energies around 1000 GeV, however, the shift caused by the terms that are summed up in the nonrelativistic expansion exceeds the theoretical error [9].

In Table I, in the last column, the ratio of the NLL nonrelativistic cross section and the $\mathcal{O}(\alpha_s)$ fixed-order cross section (with the approximation $m_t^{\rm pole} = m_t^{\rm 1S}$) for $|v| < 0.2$ is also shown. Interestingly, the higher order summations lead to correction factors ranging between about 1.7 and 1.8 that are only very weakly dependent of the c.m. energy and the Higgs mass. This fact might prove useful for rough implementations of nonrelativistic $t\bar{t}$ effects in other high energy processes.

References

[1] K. J. F. Gaemers and G. J. Gounaris, Phys. Lett. B **77**, 379 (1978); A. Djouadi, J. Kalinowski and P. M. Zerwas, Mod. Phys. Lett. A **7**, 1765 (1992); A. Djouadi, J. Kalinowski and P. M. Zerwas, Z. Phys. C **54**, 255 (1992).

[2] S. Dawson and L. Reina, Phys. Rev. D **57**, 5851 (1998) [arXiv:hep-ph/9712400].

[3] S. Dawson and L. Reina, Phys. Rev. D **59**, 054012 (1999) [arXiv:hep-ph/9808443].

[4] S. Dittmaier, M. Kramer, Y. Liao, M. Spira and P. M. Zerwas, Phys. Lett. B **441**, 383 (1998) [arXiv:hep-ph/9808433].

[5] G. Belanger *et al.*, Phys. Lett. B **571**, 163 (2003) [arXiv:hep-ph/0307029].

[6] A. Denner, S. Dittmaier, M. Roth and M. M. Weber, Nucl. Phys. B **680**, 85 (2004) [arXiv:hep-ph/0309274].

[7] Y. You, W. G. Ma, H. Chen, R. Y. Zhang, S. Yan-Bin and H. S. Hou, Phys. Lett. B **571**, 85 (2003) [arXiv:hep-ph/0306036].

[8] A. H. Hoang, arXiv:hep-ph/0204299; A. H. Hoang *et al.*, Eur. Phys. J. directC **2**, 3 (2000) [arXiv:hep-ph/0001286].

[9] C. Farrell and A. H. Hoang, to be published in Phys. Rev. D (2005) [arXiv:hep-ph/0504220].

[10] M.E. Luke, A.V. Manohar and I.Z. Rothstein, Phys. Rev. **D61**, 074025 (2000) [arXiv:hep-ph/9910209].

[11] A.V. Manohar and I.W. Stewart, Phys. Rev. D **62**, 014033 (2000) [arXiv:hep-ph/9912226].

[12] A.V. Manohar and I.W. Stewart, Phys. Rev. **D62**, 074015 (2000) [arXiv:hep-ph/0003032].

[13] A. H. Hoang and I. W. Stewart, Phys. Rev. D **67**, 114020 (2003) [arXiv:hep-ph/0209340].

[14] A. H. Hoang, A. V. Manohar, I. W. Stewart and T. Teubner, Phys. Rev. Lett. **86**, 1951 (2001) [arXiv:hep-ph/0011254]; and Phys. Rev. D **65**, 014014 (2002) [arXiv:hep-ph/0107144].

[15] A. H. Hoang, Z. Ligeti and A. V. Manohar, Phys. Rev. Lett. **82**, 277 (1999) [arXiv:hep-ph/9809423]; A. H. Hoang, Z. Ligeti and A. V. Manohar, Phys. Rev. D **59**, 074017 (1999) [arXiv:hep-ph/9811239].

[16] A. H. Hoang and T. Teubner, Phys. Rev. D **60**, 114027 (1999) [arXiv:hep-ph/9904468].

[17] A. H. Hoang, Phys. Rev. D **69**, 034009 (2004) [arXiv:hep-ph/0307376].

[18] W. Fischler, Nucl. Phys. B **129**, 157 (1977); A. Billoire, *Phys. Lett.* **B92**, 343 (1980).

[19] A. Pineda, Phys. Rev. D **66**, 054022 (2002) [arXiv:hep-ph/0110216].

[20] M. Jeżabek, J. H. Kühn and T. Teubner, Z. Phys. **C56**, 653 (1992).